Electronic Supplementary Material (ESI) for Journal of Materials Chemistry A.
This journal is © The Royal Society of Chemistry 2021

Supporting Information

Chemically Presodiated Sb with Fluoride-rich Interphase as a Cycle-stable Anode for High-energy Sodium Ion Batteries

Mengchuang Liu [‡], *Zezhou Yang* [‡], *Yifei Shen, Shuhan Guo, Junyao Zhang, Xinping Ai, Hanxi Yang, Jiangfeng Qian*[*]

Hubei Key Laboratory of Electrochemical Power Sources, College of Chemistry and Molecular Sciences, Wuhan University, Wuhan, Hubei 430072, China

[*]E-mail: jfqian@whu.edu.cn;

[‡] These authors contributed equally to this work.

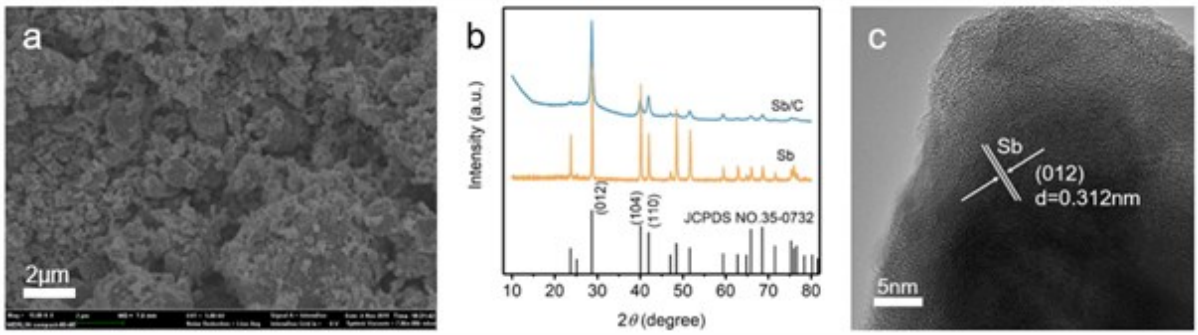

Fig. S1. Structural and morphological characterization of Sb/C sample: (a) SEM image (b) XRD pattern. (c) HR-TEM image.

Sb/C nanocomposites are prepared by mixing commercial Sb powder and super-p carbon materials using simple one-step ball milling method (for experimental details, see supporting information). The SEM image (**Fig.S1a**) shows the morphology of the sample, which is composed of several hundred nanometers (~300 nm) of irregular aggregates. The XRD pattern of the as prepared sample is shown in Figure S1b. All diffraction patterns well matched with rhombohedral phase of Sb (JCPDS no. 35-0732) and the broadened diffraction peaks are indicative of the nanosized feature of Sb after ball milling[1]. Further, high-resolution TEM image (**Fig.S1c**) more intuitively reveals Sb/C nanocomposite structural characteristics. The lattice fringes with spacing of 0.312 nm corresponding well to the (012) plane of hexagonal Sb crystal plane diffraction.[1-3]

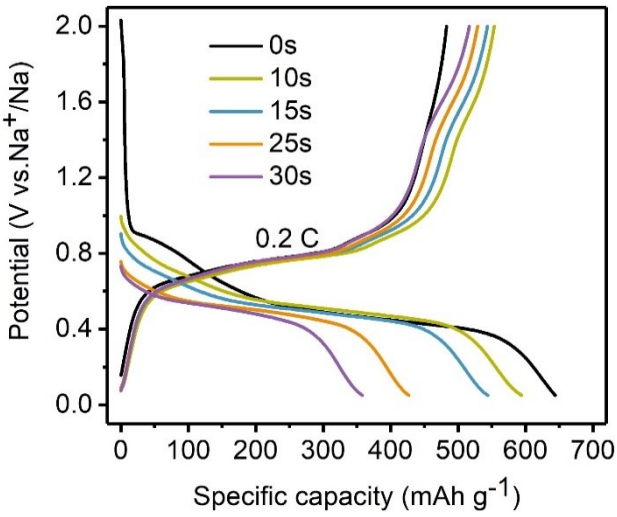

Fig. S2. The initial charging-discharging curve of the presodiated Sb/C electrodes (0, 10, 15, 25, and 30 s) at 0.2 C (1C=500 mA/g).

It is noteworthy that, compared to the non-sodiated sample (0s), the presodiated Sb samples (10-30 s) deliver slightly higher charge (Na-extraction) capacities. However, the specific charge capacities decrease as the presodiation time increasing (**Fig. S2**), which is attributed to the drastic volume expansion and pulverization of the Na_xSb alloy during the over-presodiation process. Besides, the over-sodiated Sb anode will induce massive electrolyte decomposition, resulting in a large impedance forms at the electrode/electrolyte interface, and thus a capacity decay with the prolonged sodiation time. Therefore, the presodiation time is optimized to be 15s, and the resultant Na_xSb anode reached a high ICE of ~100 % with reversible capacity of 540 mAh g^{-1}.

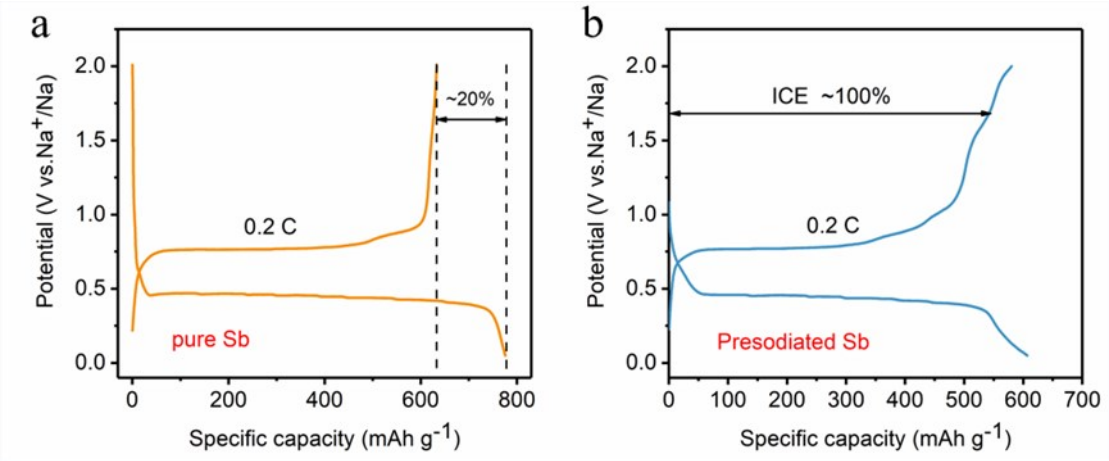

Fig. S3. The first cycle charge-discharge curves of pure Sb and presodiated pure Sb electrodes cycled at 0.2 C rate (1C=500 mA g-1).

In order to exclude the interference of carbon components, we conducted control tests on pure Sb powder. As shown in **Fig. S3**, the pure Sb electrode shows a low initial columbic efficiency of ~80% in the first cycle, which was elevated to nearly 100% after presodiation treatment for 15s. These results undoubtedly demonstrate the effectiveness of our presodiation strategy to Sb alloying anode.

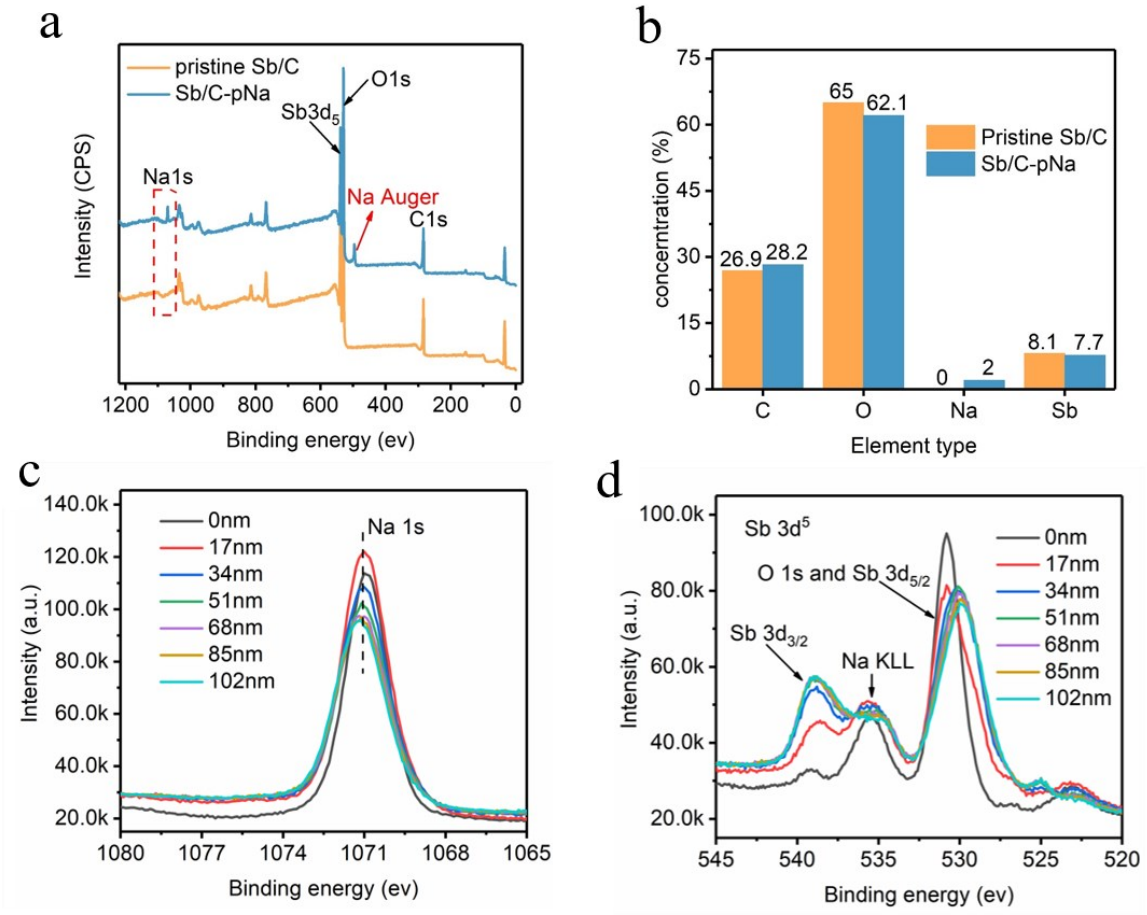

Fig. S4. XPS characterization of the pristine Sb and presodiated Sb-pNa materials: (a) XPS full spectrum and (b) atomic ratio of elements. (c-d) XPS depth profiling on the presodiated Sb-pNa electrode as a function of the etching thickness. (c)Na 1s spectrum and (d)Sb 3d5 spectrum. The Ar-ion etching rate is about 17.12 nm/min based on the calibration of SiO_2.

XPS measurements interlaced with Ar-ion etching was conducted to evaluate the reaction depth within the Sb particle after presodiation treatment. The etching rate is about 17.12 nm/min based on the calibration of SiO_2. As seen in **Fig. S4 c** and **d**, after etching for ~102 nm (6 min), we can still observe pronounced Na signals element in Na1s and Sb 3d spectra. These results suggested that the chemical Na^+ pre-insertion reaction occurs to form homogeneous Na_xSb alloy (as illustrated in Fig. 1 in the main text), rather than merely surface reaction to generate a core-shell type $Sb@Na_xSb$ composite.

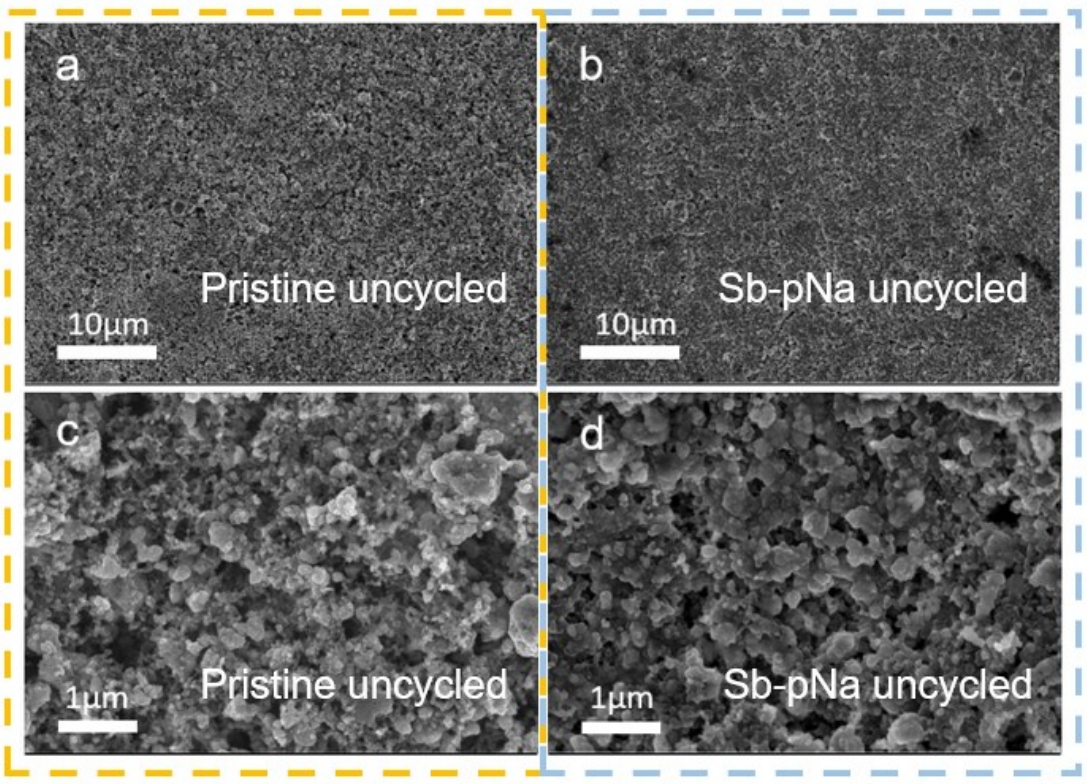

Fig. S5. SEM characterization on the uncycled pristine Sb electrode and presodiated Sb-pNa electrode.

Scanning electron micrography (SEM) tests were conducted to reveal the structure and morphology changes after presodiation treatment. As shown in **Fig. S5** , the mean particle size of Sb-pNa power (~400 nm) are larger than that of pristine Sb electrode (~300 nm), suggesting a volume expansion due to Na alloying reaction after presodiation treatment.

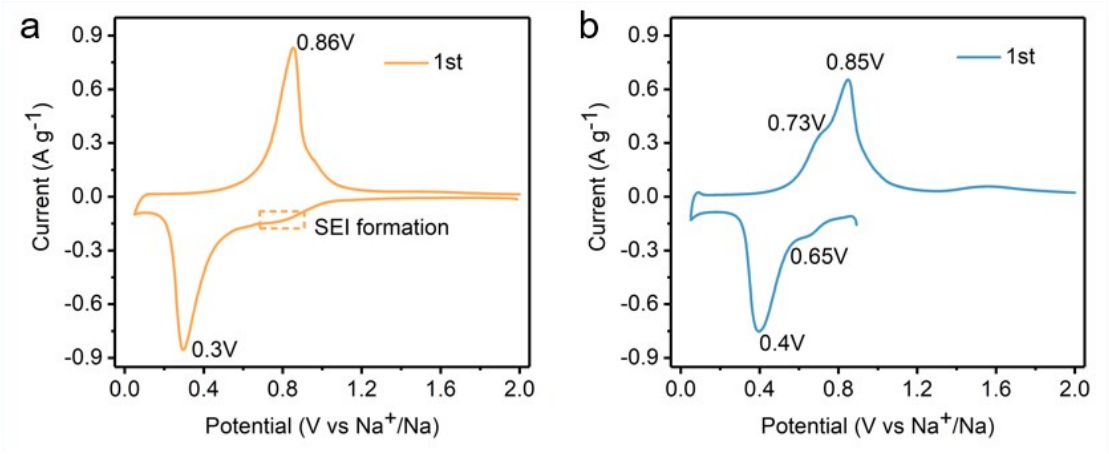

Fig. S6. Cyclic voltammetry curves of (a) pristine Sb electrode and (b) Sb-pNa electrode during the initial cycles at a scan rate of 0.1 mV s^{-1}.

Fig. S6 compares the CV profiles of pristine Sb and presodiated Sb-pNa electrodes at a scan rate of 0.1 mV/s between 0.05 and 2.0 V. The pristine Sb electrode (**Fig. S6a**) displays a broad irreversible peak at ~0.8 V in the first cathodic scan owing to electrolyte decomposition to form SEI layer. The subsequent 0.3 V cathodic and 0.86 V anodic peaks correspond to Na^+ alloying/dealloying reactions on Sb matrix ($Sb \rightarrow Na_3Sb$).

Quite differently, the CV curve of Sb-pNa anode did not show the irreversible reduction peak due to the decomposition of electrolyte (**Fig. S6b**), suggesting that there exists an SEI layer already on Sb-pNa electrode. In addition, the Sb-pNa electrode exhibits a smaller peak separation between cathodic (0.4V) and anodic (0.85V) potentials, implying a faster electrochemical reaction kinetics than that of pristine Sb.

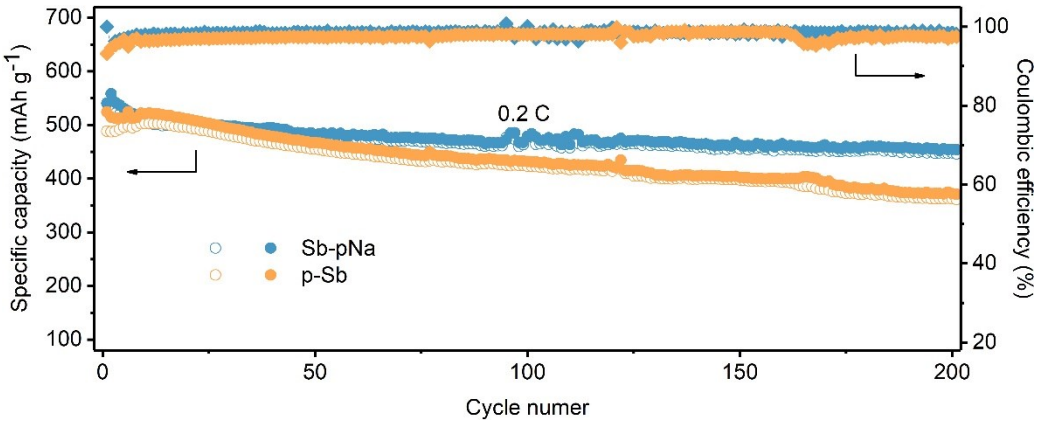

Fig. S7. Cycling performance and coulombic effficiencies of Na|| Sb cell (a) and Na||Sb-pNa half cells at 0.2 C.

Fig. S7 compares the cycling stability of pristine Sb and presodiated Sb-pNa electrodes cycled at a low rate of 0.2 C. The Sb-pNa shows a retention of 85 % after 200 cycles, whereas pristine Sb remains only 70% of its initial capacity over the same cycles. It should be pointed that the capacities fluctuations at about 100 cycles for the Sb-pNa electrode might be attributed to the fluctuation of the test temperature. In addition, the average coloumbic efficiency of Sb-pNa anode over 200 cycles is ~98.4%, higher than that of ~97.9% for pristine Sb anode. These results suggest that the presodiation treatment can effectively suppress the growth of resistive SEI film on electrode surface, thus enabling a rather stable cycling performance.

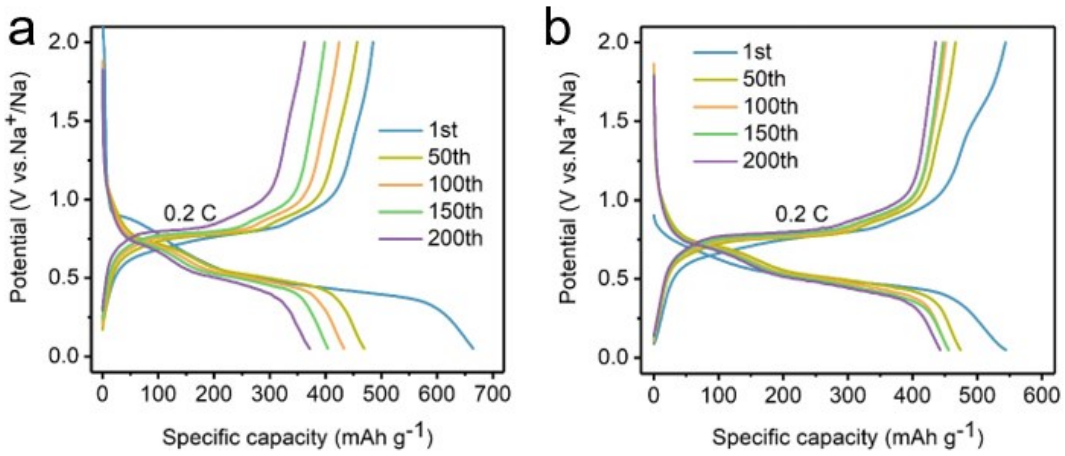

Fig. S8. Voltage profiles of Na|| Sb cell (a) and Na||Sb-pNa cell (b) at selected cycles during cycling at 0.2 C.

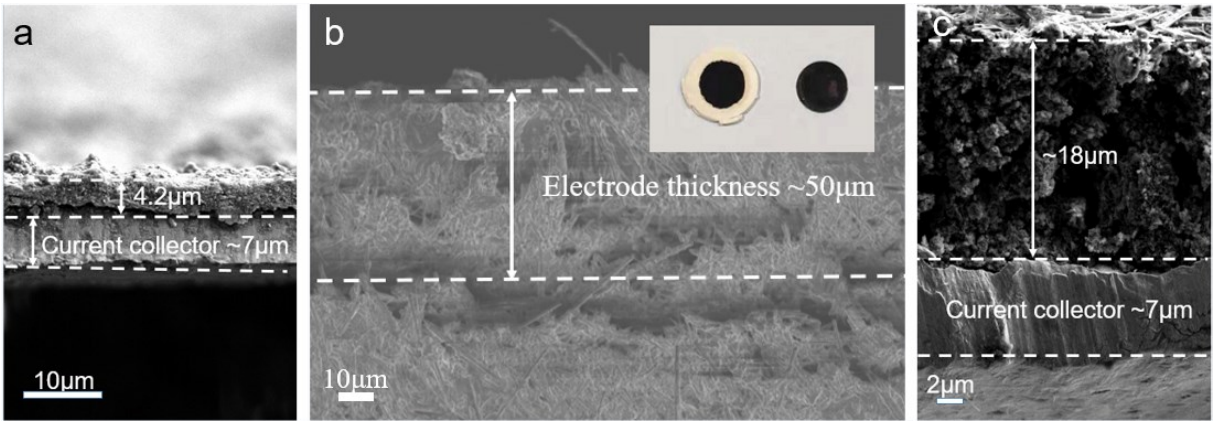

Fig. S9. The cross-sectional SEM images of (a) uncycled pristine Sb electrode, (b) pristine Sb electrode after 300 cycles at 4 C and (c) Sb-pNa electrode after 300 cycles at 4 C.

As can be seen from the cross-sectional SEM images of the cycled electrodes in **Fig. S9**, pristine Sb electrode suffers more than tenfold volume expansion from 4.2 μm to 50 μm after 300 cycles, and some Sb particles even peeled off from the current collector. In contrast, the Sb-pNa electrode only expands to 18 μm, and keep tight adhesion to the current collector after 300 cycles.

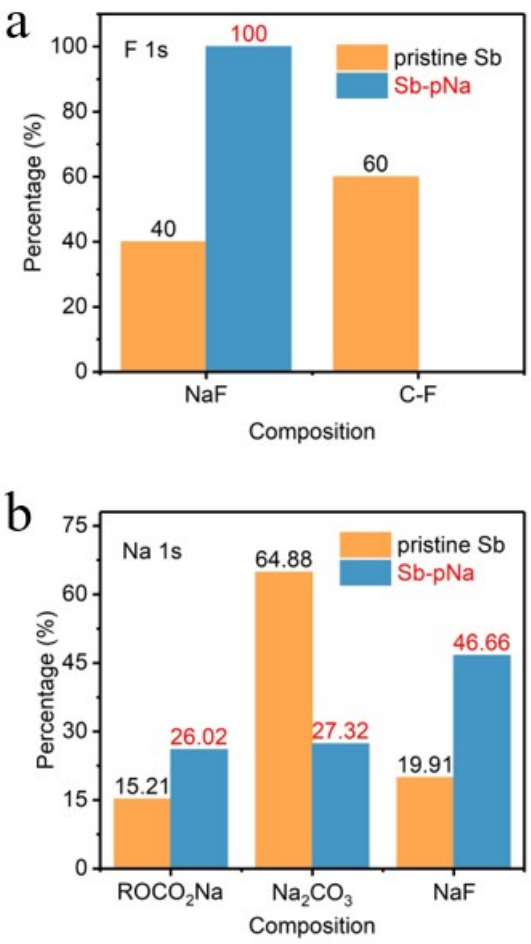

Fig. S10. The decomposition products proportion of solvent reduction in F1s (a) and Na1s (b) spectra.

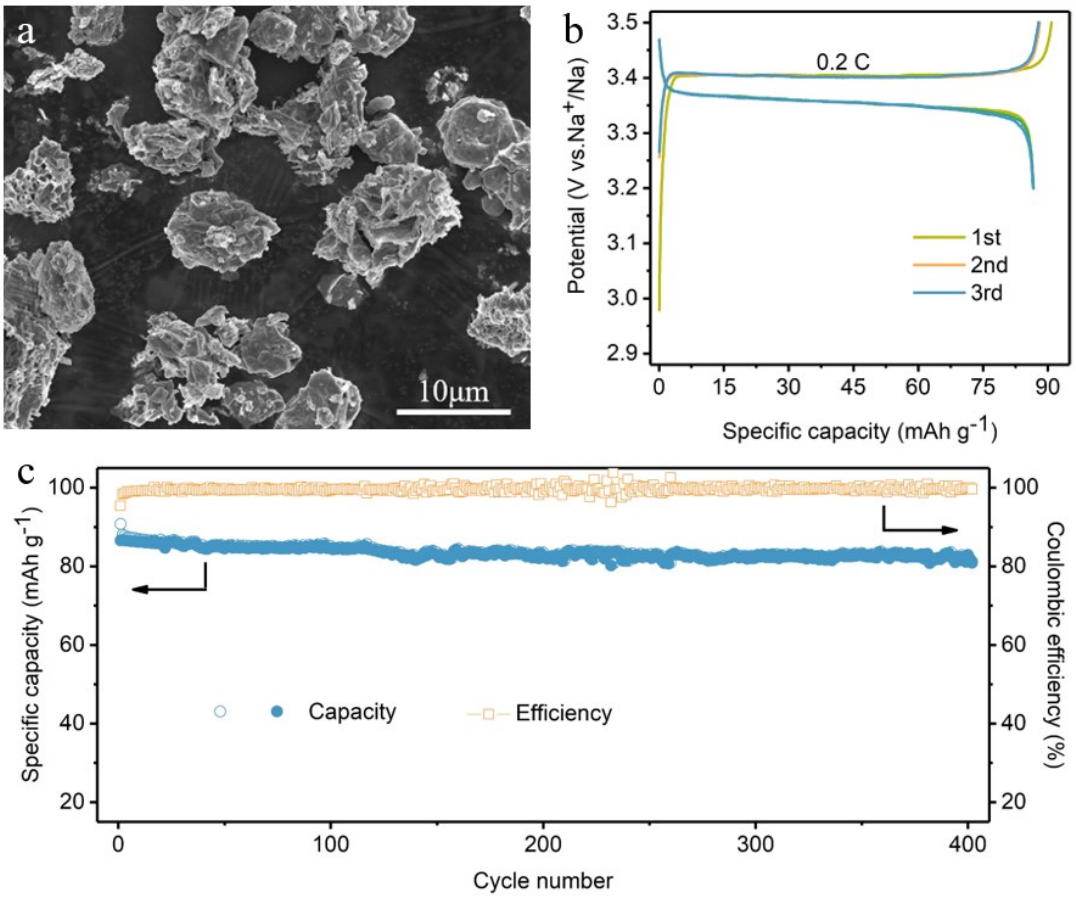

Fig.S11. (a)SEM images of $Na_2V_3(PO_4)_2$@C sample. Electrochemical property of $Na_2V_3(PO_4)_2$@C cathode: (b) voltage profiles of the first three cycles at 0.2 C and (c) long cycling performance at 0.2C (1C=120 mA g^{-1}).

The morphological feature and electrochemical performances of $Na_2V_3(PO_4)_2$ sample were revealed in **Fig.S11**. As shown in Figure S 9b**,** the constant current charge-discharge curves appear two obvious voltage plateaus at 3.3/3.4V, corresponding to the reversible redox reaction of V^{3+}/V^{4+} ($Na_2V_3(PO_4)_2 \leftrightarrow NaV_3(PO_4)_2 + Na^+ + e^-$).[3, 4] In addition, the high capacity retention rate of 96% after 400 cycles indicates the NVP electrode has excellent cycling stability.

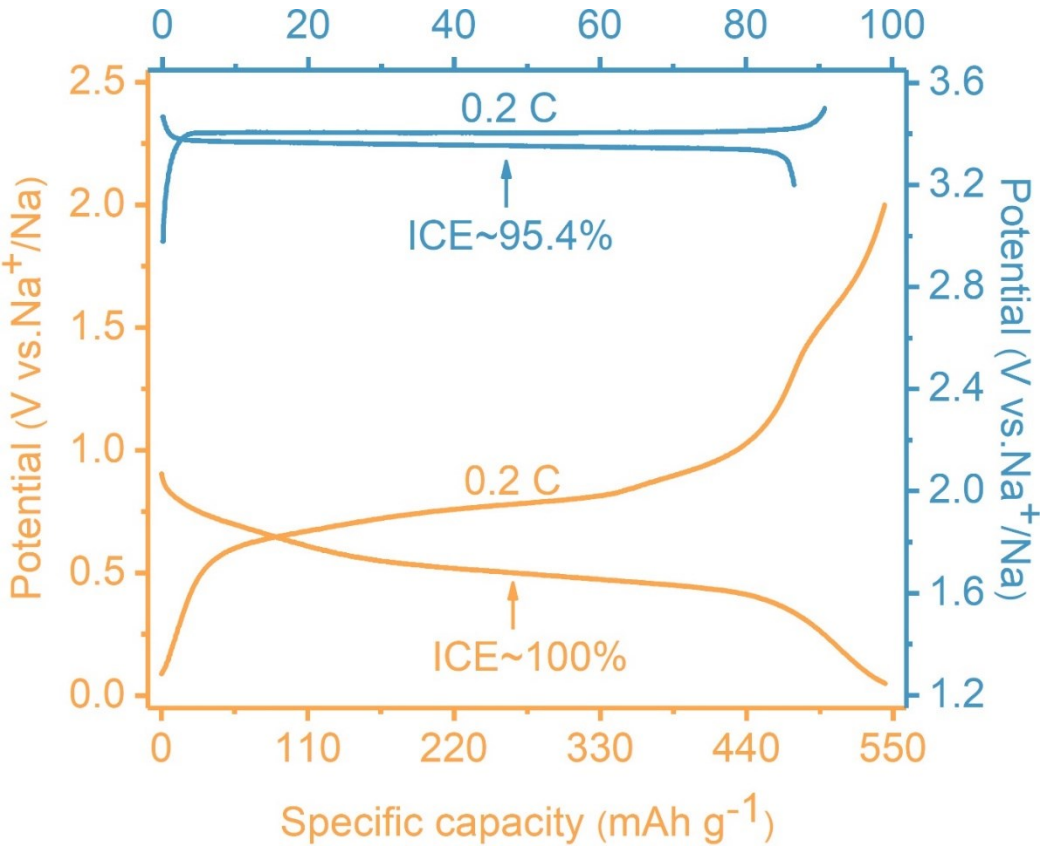

Fig. S12. Initial voltage curve of Sb-pNa negative and NVP positive electrodes at 0.2C (1 C=500 mA g^{-1}), respectively.

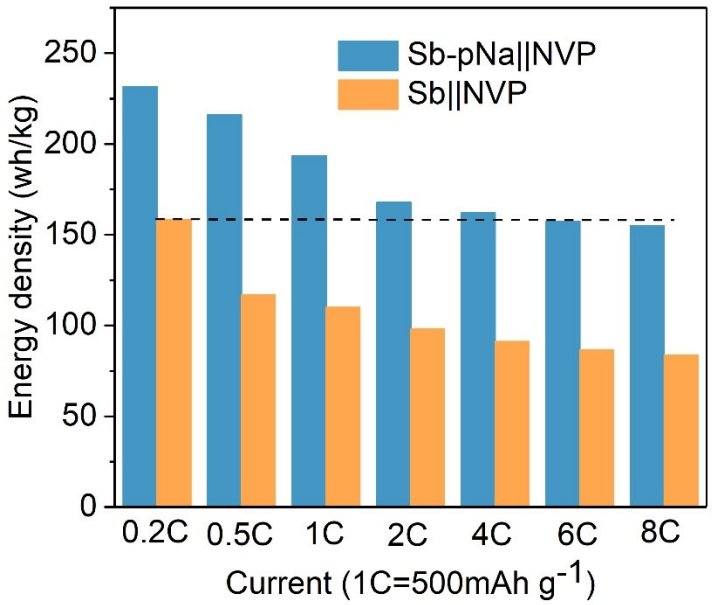

Fig. S13. The energy density comparison of both full-cells at 0.2-8 C.

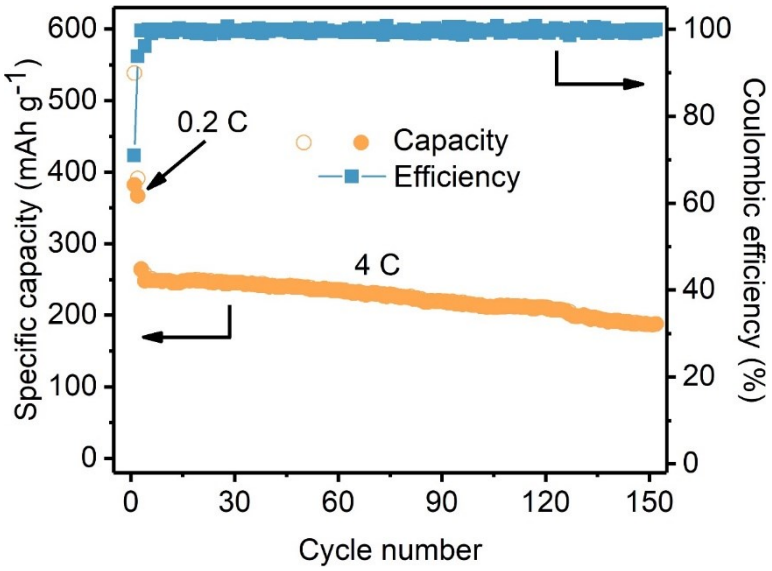

Fig. S14. Long cycling performance of Sb||NVP full cell at 4C.

Tab. S1. A survey of the initial coulomb efficiency (ICE) of Sb anodes in SIBs.

Nanostructure	ICE (%)	Ref
electrospun nanowire	55%	5
	56%	2
hollow Sb@C Yolk-Shell Spheres	60.3%	6
Yolk-shell structured Sb@C	69%	7
pomegranate Sb@C yolk-shell microspheres	~60%	8
multi-shell hollow	55	9
Nanoporous-antimony	~65%	10
Highly uniform Sb nanotubes	71%	11
Sb@C coaxial nanotubes	50%	12

Tab. S2. Fitted values for the equivalent circuit elements in Fig. 5

	Rs/(Ω)		**R_{SEI}/(Ω)**		**R_{CT}/(Ω)**	
	Sb	Sb-pNa	Sb	Sb-pNa	Sb	Sb-pNa
1st	13.09	5.18	210.7	60.87	392.8	118.5
2nd	15.87	5.39	275.2	56.4	379.3	143.6
3rd	12.95	5.13	217.3	47.8	402.4	135
5th	10.8	4.88	176.3	39.5	397	109.7

Tab. S3. A survey of the electrochemical properties of sodium ion full cells reported in literatures.

Cathode-Anode	Potential(V)	ICE (%)	Cycle performance	Energy density (Wh/kg)	Ref.
NVP-Sb	2.61	95.5	70%(150 cycles)	232	This work
NVP-Sb	2.7	---	74% (100 cycles)	205	13
NVPF-Sb	3.0	87.6	80% (50 cycles)	---	14
NVP-SnS	2.2	72.4	85.5% (300 cycles)	99.8	15
$Na_{0.8}Li_{0.12}Ni_{0.22}Mn_{0.66}O_2$-$SnS_2$	2.5	63.6	74% (50 cycles)	191	16
NVP-AC	1.7	---	80% (200 cycles)	186	17
NVP-NVP	1.7	77	92.2%(100cycles)	71.2	18
NVP-graphene	2.7	94.3	77.1% (200 cycles)	123	19
NVP-NVP	1.7	---	77% (100 cycles)	150	20
NVP-NVP	1.8	85	81% (280 cycles)	162	21
NVP-CPNW	2.6	68.3	38%(200 cycles)	104	22
NVP-MoS_3	1.8	68.3	84%(100 cycles)	100.8	23
NVPF-NTP	1.5	70	71%(1000 cycles)	73	24
NVOPF-NTP	1.7	---	86%(1800 cycles)	45.4	25
NVP-HC	3.26	70.6	89.2% (300 cycles)	143.7	26
$Na_{0.9}[Cu_{0.22}Fe_{0.30}Mn_{0.48}]O_2$-HC	3	92.9	87.6%(20 cycles)	240	27

References

1. J. Qian, Y. Chen, L. Wu, Y. Cao, X. Ai and H. Yang, *Chem. Commun.*, 2012, **48**, 7070-7072.
2. L. Wu, X. Hu, J. Qian, F. Pei, F. Wu, R. Mao, X. Ai, H. Yang and Y. Cao, *Energy Environ. Sci.*, 2014, **7**, 323-328.
3. Y. Fang, L. Xiao, X. Ai, Y. Cao and H. Yang, *Adv. Mater.*, 2015, **27**, 5895-5900.
4. Y. Jiang, Z. Z. Yang, W. H. Li, L. C. Zeng, F. S. Pan, M. Wang, X. Wei, G. T. Hu, L. Gu and Y. Yu, *Adv. Energy Mater.*, 2015, **5**, 1402104.
5. Y. Zhu, X. Han, Y. Xu, Y. Liu, S. Zheng, K. Xu, L. Hu and C. Wang, *ACS Nano*, 2013, **7**, 6378-6386.
6. J. Liu, L. Yu, C. Wu, Y. Wen, K. Yin, F. K. Chiang, R. Hu, J. Liu, L. Sun, L. Gu, J. Maier, Y. Yu and M. Zhu, *Nano Lett.*, 2017, **17**, 2034-2042.
7. J. Song, P. Yan, L. Luo, X. Qi, X. Rong, J. Zheng, B. Xiao, S. Feng, C. Wang, Y.-S. Hu, Y. Lin, V. L. Sprenkle and X. Li, *Nano Energy*, 2017, **40**, 504-511.
8. J. Song, D. Xiao, H. Jia, G. Zhu, M. Engelhard, B. Xiao, S. Feng, D. Li, D. Reed, V. L. Sprenkle, Y. Lin and X. Li, *Nanoscale*, 2018, **11**, 348-355.
9. F. Xie, L. Zhang, Q. Gu, D. Chao, M. Jaroniec and S.-Z. Qiao, *Nano Energy*, 2019, **60**, 591-599.
10. Y. Z. Li, K. Yan, H. W. Lee, Z. D. Lu, N. Liu and Y. Cui, *Nat. Energy*, 2016, **1**, 8.
11. Y. Liu, B. Zhou, S. Liu, Q. Ma and W. H. Zhang, *ACS Nano*, 2019, **13**, 5885-5892.
12. Z. M. Liu, X. Y. Yu, X. W. D. Lou and U. Paik, *Energy Environ. Sci.*, 2016, **9**, 2314-2318.
13. H. C. Gao, W. D. Zhou, K. Park and J. B. Goodenough, *Adv. Energy Mater.*, 2016, **6**.
14. J. Z. Guo, P. F. Wang, X. L. Wu, X. H. Zhang, Q. Yan, H. Chen, J. P. Zhang and Y. G. Guo, *Adv. Mater.*, 2017, **29**, 1701968.
15. X. Xiong, C. Yang, G. Wang, Y. Lin, X. Ou, J.-H. Wang, B. Zhao, M. Liu, Z. Lin and K. Huang, *Energy Environ. Sci.*, 2017, **10**, 1757-1763.
16. B. Qu, C. Ma, G. Ji, C. Xu, J. Xu, Y. S. Meng, T. Wang and J. Y. Lee, *Adv. Mater.*, 2014, **26**, 3854-3859.
17. S. Li, Y. Dong, L. Xu, X. Xu, L. He and L. Mai, *Adv. Mater.*, 2014, **26**, 3545-3553.
18. T. F. Hung, W. J. Cheng, W. S. Chang, C. C. Yang, C. C. Shen and Y. L. Kuo, *Chem. Eur. J*, 2016, **22**, 10620-10626.
19. X. Cao, A. Pan, S. Liu, J. Zhou, S. Li, G. Cao, J. Liu and S. Liang, *Adv. Energy Mater.*, 2017, **7**.
20. C. Zhu, P. Kopold, P. A. van Aken, J. Maier and Y. Yu, *Adv. Mater.*, 2016, **28**, 2409-2416.
21. Y. Zhang, H. Zhao and Y. Du, *J. Mater. Chem. A*, 2016, **4**, 7155-7159.
22. M. P. Fan, Y. Chen, Y. H. Xie, T. Z. Yang, X. W. Shen, N. Xu, H. Y. Yu and C. L. Yan, *Adv. Funct. Mater.*, 2016, **26**, 5019-5027.
23. H. Ye, L. Wang, S. Deng, X. Zeng, K. Nie, P. N. Duchesne, B. Wang, S. Liu, J. Zhou, F. Zhao, N. Han, P. Zhang, J. Zhong, X. Sun, Y. Li, Y. Li and J. Lu, *Adv. Energy Mater.*, 2017, **7**.
24. Q. Liu, X. Meng, Z. Wei, D. Wang, Y. Gao, Y. Wei, F. Du and G. Chen, *ACS Appl. Mater. Interfaces*, 2016, **8**, 31709-31715.
25. P. R. Kumar, Y. H. Jung, J. E. Wang and D. K. Kim, *J. Power Sources*, 2016, **324**, 421-427.
26. X. Jiang, X. Liu, Z. Zeng, L. Xiao, X. Ai, H. Yang and Y. Cao, *iScience*, 2018, **10**, 114-122.
27. X. Liu, Y. Tan, T. Liu, W. Wang, C. Li, J. Lu and Y. Sun, *Adv. Funct. Mater.*, 2019, **29**, 1903795.